

SIMULATION ASSISTED HIGH-RESOLUTION PSI ANALYSIS

A. Schunert^{a,*}, T. Balz^b, K. Liu^b, M.S. Liao^b, U. Soergel^a, JD Wegner^a

^a Institute of Photogrammetry and GeoInformation, Leibniz Universität Hannover, Hannover, Germany

^b State Key Laboratory of Information Engineering in Surveying, Mapping and Remote Sensing, Wuhan University, Wuhan, China

Commission VII

KEY WORDS: SAR, Radar, PSI, Simulation, TerraSAR-X

ABSTRACT:

Since the first demonstration of the potential of the differential SAR interferometry in the early 1990s a lot of effort has been made to accurately estimate ground deformation with imaging radar sensors. This led to the invention of the Persistent Scatterer Interferometry (PSI) in the late 1990s. PSI enables the estimation of ground deformation for a set of temporally stable radar reflectors, the so called PS, with millimeter accuracy. The main advantage compared to methods commonly used for ground deformation monitoring like GPS is the possibility to cover large areas very economically. One of the main drawbacks is the opportunistic sampling of the target area, which is mainly governed by the distribution of stable radar reflectors within the scene. Besides problems caused by undersampling the main issue is due to the fact, that the real world feature related to a PS is usually not known. This makes the interpretation of the results particularly difficult. While the assignment of these real world features is very difficult in the case of ERS like sensors, modern high resolution SAR sensors like TerraSAR-X (TSX) render this task possible. We investigate the use of SAR simulation to match real world features with PS extracted from a TSX stack acquired over the city of Berlin Germany. The simulation is based on a 3D city model of the area around the Potsdamer Platz, Berlin.

1. INTRODUCTION

With the help of the Persistent Scatterer Interferometry (PSI) surface deformation can be estimated with millimetre accuracy. The sampling of the phenomenon under investigation is thereby determined by the backscattering behaviour of the scene at hand since only temporally stable radar targets can be used.

Despite the high accuracy of the PS results, their interpretation is quite difficult due to the fact that it is unknown a priori which real world feature appertains to a given PS. If the aim of a PS analysis is, for instance, the determination of ground deformation, building movements due to thermal dilation or settling may be confused with the signal of interest. This is especially a problem in case of ERS-like sensors, where a mapping of PS to single buildings is almost impossible. Against this the modern high resolution SAR sensors like TerraSAR-X (TSX) provide a resolution, which is sufficient to recognize even small features of buildings. We investigate the joint use of PSI and SAR simulation for determining the physical cause of PS. Therefore, a stack of 20 TSX high resolution spotlight images, acquired over the city of Berlin is used for the PSI analysis. The images exhibit a ground range resolution of 1.2 meter.

For the simulation a 3D city model was used, which was derived from airborne laserscanning data.

2. PERSISTENT SCATTERER INTERFEROMETRY

The PSI technique is an extension of the classical SAR interferometry, to mitigate the problems due to temporal

decorrelation and atmospheric disturbances. Temporal decorrelation arises through changes in the backscattering behaviour of a resolution cell over time, which can be alleviated by restricting the analysis to a set of temporally stable radar targets, referred to as Persistent Scatterers (PS).

Tropospheric water vapour influences the refraction coefficient and therefore the velocity of light. Hence, different atmospheric conditions at the times of master and the slave image acquisitions may result in an undesired term of the interferometric phase caused different path delay. This term has to be removed to estimate topography or deformation with reasonable accuracy. Within the framework of PSI this is usually done with the help of a stack of interferograms.

The first step of a PSI analysis is to extract a set of PS candidates. This can be achieved in several ways. We used the amplitude dispersion index introduced by Ferretti *et al.* (2001) for that purpose, which is computed for every image pixel as follows:

$$D_A = \frac{\sigma_A}{m_A} \quad (1)$$

The variables σ_A and m_A denote the standard deviation and the mean of the amplitude of every pixel estimated over time, respectively. As shown in Ferretti *et al.* (2001) the amplitude

*corresponding author



Figure 1. Phase of one interferogram of the stack overlaid on the mean amplitude image.

dispersion is a good estimate of a scatterer's phase stability if the scatterer's signal exhibits a high signal to noise ratio. However, the quality of resolution cells with low signal to noise ratio is overestimated, leading to the necessity to set a quite strict threshold in the beginning to avoid false positives. We choose the amplitude dispersion threshold to be 0.2, to have a negligible number of those. Additionally, groups of adjacent PS are thinned out by just considering the best PS in a 4 connectivity neighbourhood. The distribution of the PS is illustrated in Figure 1 overlaid on the mean amplitude image of the TSX data stack. The colours represent phase values of one interferogram.

The PS density is about 20 000 PS per km², which is quite low compared to PS densities found by Bamler *et al.* (2009), which can be explained by the quite strict selection criteria. It can be seen, that many PS reside at building façades. We expect those to be generated by structures such as windows or balconies. For some PS it is not clear if they are caused by scattering at the façade or the roof of a building since both target areas may be mapped to the same image position.

After the initial selection signal processing is carried out for the candidate set, in order to discriminate between the respective contributions forming the interferometric phase, which can be modelled according to Hooper *et al.* (2007) as

$$\psi_{\text{int},x,i} = W \left\{ \varphi_{\text{def},x,i} + \varphi_{\text{atm},x,i} + \Delta\varphi_{\text{orb},x,i} + \Delta\varphi_{\theta,x,i} + \varphi_{n,x,i} \right\} \quad (2)$$

where

- $\varphi_{\text{def},x,i}$ contains the phase due to the surface movement projected to the sensors line of sight;
- $\varphi_{\text{atm},x,i}$ is the phase due to different atmospheric states during master and slave acquisitions;

- $\Delta\varphi_{\text{orb},x,i}$ denotes the phase emerging from errors in the satellites orbit determination;
- $\Delta\varphi_{\theta,x,i}$ is called look angle error and is caused by two effects. These are contributions due to residual topographic phase components and deviation of the pixels phase centre from its geometric centre in range direction. The latter effect is considered to be negligible because of the high resolution of the data. The residual topography terms the vertical distance between the reference surface and the PS. In this case the WGS 84 ellipsoid is used as a reference surface.
- $\varphi_{n,x,i}$ is the phase noise which is largely caused by changes of the pixels reflectivity with time and look angle;

In this paper we are just interested in estimating the residual topography to get information about a scatterer's 3D position. We use a standard PS approach following the ideas of Ferretti *et al.* (2000) and Liu *et al.* (2009) here. The phase due to deformation is modelled as a linear function of time. Atmosphere and effects related to orbit errors are assumed to be low pass components in space. Finally residual topographic phase is a linear function of the effective spatial baseline separating every interferometric image pair.

In a first step phase differences between neighbouring PS are calculated, which mainly cancels out the phase caused by atmosphere and orbit errors. Thereby the neighbourhood is given by a Delaunay triangulation. For every phase difference between two PS at positions x and y velocity and height increments denoted by v_{xy} and H_{xy} respectively are calculated using a coherence maximisation approach (see for instance Liu *et al.* (2009)), which can be stated as

$$\gamma_{xy} = \max_{v_{xy}, H_{xy}} \frac{1}{N} \left| \sum_{i=1}^N e^{j \left(\psi_{\text{int},x,i} - \frac{4\pi}{\lambda} \frac{B_i^\perp}{R \sin \theta} H_{xy} - \frac{4\pi}{\lambda} T_i v_{xy} \right)} \right| \quad (3)$$

where

- B_i^\perp is the spatial baseline,
- T_i is the temporal baseline,
- λ is the wavelength of the sensor,
- R is the distance from sensor to target,
- θ is the off nadir angle of the radar.

The term γ_{xy} denotes the so called temporal coherence factor and serves as quality measure to evaluate how good the observations fit the assumed model. Results having a value below 0.7 are removed before the next step.

In order to calculate the PS height from the height increment a overdetermined system of linear equation has to be solved, which is done by means of an iteratively reweighted least squares approach. Within the inversion of this system remaining gross errors are removed from the data (see Liu *et al.* (2009) for reference).

The result is a height and a velocity estimate for every PS relative to a reference PS in the scene. While the height can be estimated with submeter accuracy, accuracies of the subsidence rate are in the order of few millimetres per year. The geocoded PS overlaid to the 3D model used for simulation are shown in Figure 2.

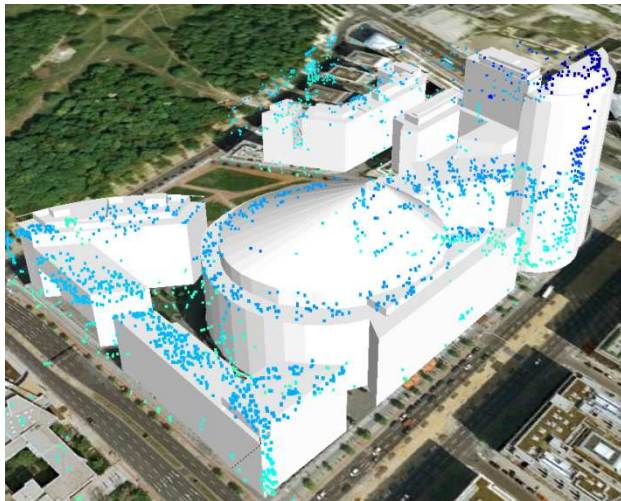


Figure 2. 3D model of the Sony-Center overlaid with PS

3. SAR SIMULATION

3.1 3D city model

The 3D city model, which is the basis for simulation was derived from airborne laser scanning data. We used the free software tool sketchup to reconstruct surfaces from the point cloud. The whole procedure was conducted manually, i.e., no meshing algorithms were used. The result is displayed in Figure 2 together with the geocoded PS.

3.2 Fast ray-tracing SAR simulation approach

SAR simulations aiming at precise prediction of PS positions require high geometrical correctness, whilst radiometric features are less important. According to the classification of Franceschetti *et al.* (1995) SAR simulation systems can be differentiated into raw data and image simulation systems. For our application SAR image simulation systems are feasible, because the focus is on the geometry. To ensure geometrical correctness together with computational efficiency, we use ray-tracing for our SAR simulation. Ray-tracing based SAR simulations can simulate the SAR geometry precisely, while keeping the amount of new software to be coded small by reusing and editing ray tracing tools developed for computer graphics applications (see e.g. Auer *et al.* 2010).

In our experiments we use a SAR simulator prototype based on the GPU ray-tracing library Optix™ from NVIDIA (2009). Optix™ traces the rays by using the tremendous calculation speed of modern graphics processing units (GPU), allowing for real-time or near real-time ray tracing. By adjusting the library, a real-time SAR simulator can be developed.

In this way, a fast, widely used, and extensively tested ray tracing library can be applied, which speeds up the developing process.

The simulation system we used was tailored for airborne SAR systems. Simulating TerraSAR-X data required some adjustments. The distance between the sensor and the objects on the ground are much larger in the spaceborne case, which caused troubles due to the limits of the 32-bit floating point values used in data processing. The real distances were just too large to be simulated. By setting the simulated sensor distance to around 200 km, we believe we found an acceptable compromise. The differences in the simulated geometry due are rather small, especially compared to the errors in the simulated building models.

The radiometric simulation is based on the model of Zribi *et al.* (2006) model, which does not exactly fit for urban environments. Because for our application the simulated radiometry does not need to be very accurate, we believe this is an acceptable simplification.



Figure 3. Mean amplitude image of the data stack

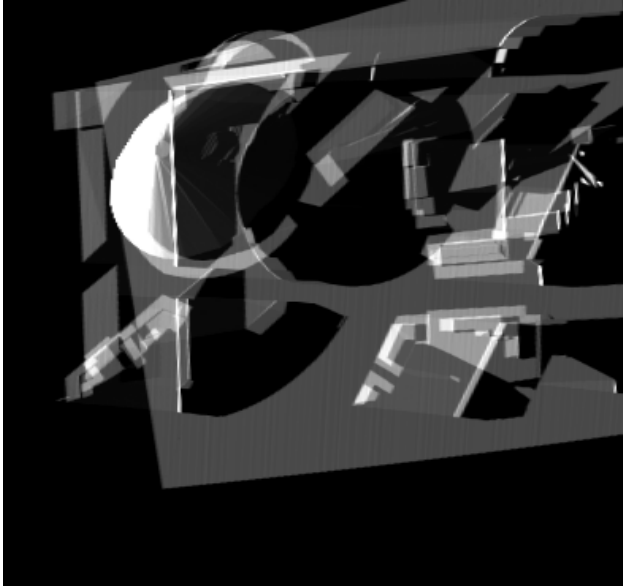


Figure 4. Simulated image containing single and double bounce contributions

3.3 SAR simulation for PSI analysis

In order to compare the PS extracted from the data stack with the results of the simulation, the simulated image is warped to the geometry of the data stack. This is necessary due to different coordinate systems of the simulated scene and the real scene, and because of small geometrical errors caused by the simulation of an airborne sensor system.

We applied an affine transformation for the warping procedure. The coefficients of this model were estimated using a number of six tie points distributed over the whole simulated scene. The result is displayed in Figure 3 and Figure 4. The mean amplitude image of the stack is displayed in Figure 3, while the simulated scene containing single and double bounce contributions is shown in Figure 4. It can be clearly seen, that the main structures of the buildings are reproduced by the simulation.

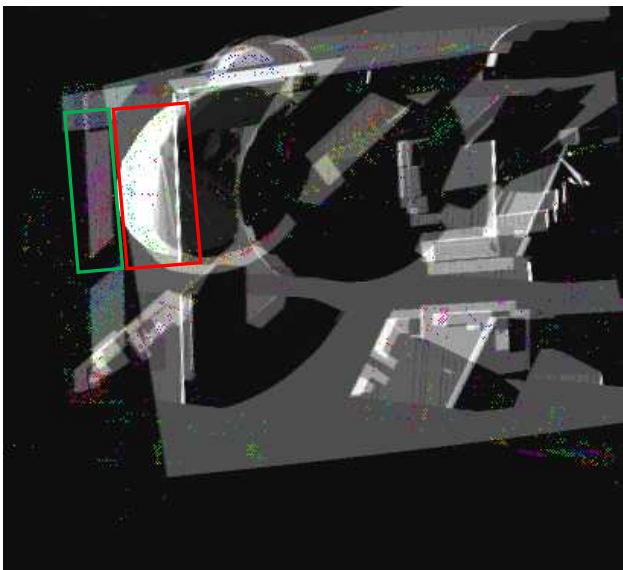


Figure 5. Simulated image overlaid with PS

Within the simulation we can distinguish between single- and double-bounce reflections. Locations of double-bounce between the dihedral corner reflector spanned by building walls and the ground in front are clearly visible in the real and the simulated SAR image.

However, the details of the façades are not visible, even facade structures which cause very strong reflections are often too small to be represented in the 3D model.

The PS set superimposed on the simulated image is shown in Figure 5. It is clearly visible, that besides some geometrical inconsistencies (see skyscraper at the top of the image) the PS set matches fairly well with the simulated image. On the other hand the main problem of the whole approach shows up. Since most of the PS are generated by small scale building features (like the above mentioned balconies and windows), which are not modelled in the simulation, detailed analysis of the physical nature of the PS is virtually impossible.

The whole situation can be best illustrated by considering the part of Figure 5 marked by the red rectangle. In this area lots of PS appear, but the simulation just indicates a homogeneous area. These PS reside mainly on the roof of the round shaped building in the centre of the building block, as can be seen from the height data in

Figure 2. An oblique view aerial image shown in Figure 6 reveals the structures leading to this group of PS. First of all, a lot of hardware, which may be used for ventilation purposes, is visible. Additionally, a metallic frame surrounds the dome-like part of the roof in Figure 6. Both types of structures are likely to produce PS, but are not contained in the 3D model used for simulation. Therefore an assignment of the respective PS to these building features using the shown simulation results is hardly possible.

For simulating these structures we would need a 3D building model reconstructed from terrestrial laser scanning or close-range photogrammetry. Less accurate, but for some applications still acceptable, would be models reconstructed using façade grammars describing the façade (Becker 2009). In this way, models of simple standardized buildings can be generated without using high-resolution laser scanning data or close-range photogrammetry.

The Sony-Center and the surrounding buildings used in our experiments are not standardized buildings easily representable in a façade grammar. We also do not have high resolution façade data. Therefore, we couldn't reconstruct a 3D building model in the required quality.

However, the simulation is useful to retrieve information about the PS within the green box. We know that virtually all scattering within this area is due to the roof of the building, which encompasses the round shaped one.



Figure 6. Oblique view aerial image

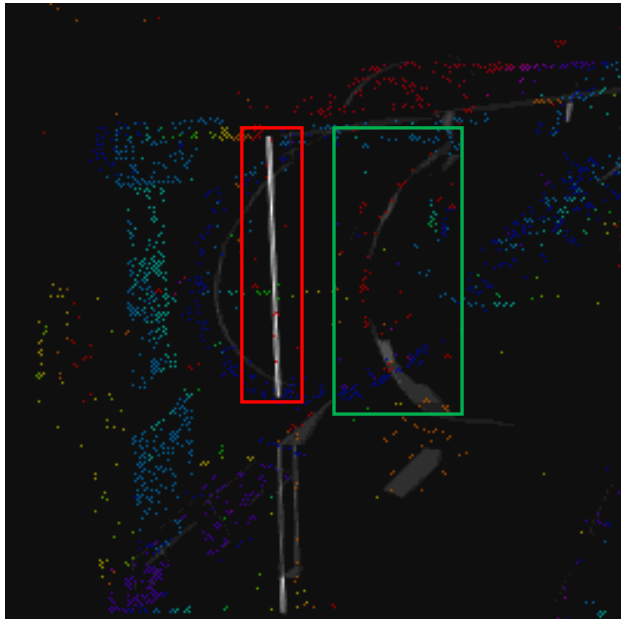


Figure 7. Simulated double bounce reflections overlaid with PS

Therefore, it is reasonable to assume that the PS are caused by structures on this roof and not by scatterers located at the upper part of the facade. This assumption is verified by the estimated height of the PS (see Figure 2).

It is furthermore possible to assess PS located on double bounce lines induced by large scale building features (e.g. curb-to-wall scattering). These are displayed in Figure 7. The PS heights arranged in five meter classes are overlaid to simplify the discrimination of PS on and off the double bounce lines. It is apparent, that the PS densities on the double bounce lines are not always as high as one may expect due to the strong backscattering. An example is marked by the red box in Figure 7, where there are hardly any PS resident (PS coloured in light red). In contrast to that, there are lots of PS on the double bounce feature marked by the green box. The reason for that is to be investigated.



Figure 8. Oblique view aerial image of the DB-Tower

As can be seen from the oblique view aerial image in Figure 6 the virtue of the respective façades differ in terms of material and geometry.

Finally it is remarkable, that there are almost no PS at the façades visible in Figure 6, which is apparent from Figure 2 and Figure 5. This is surprising, since there are usually plenty of PS at building fronts oriented towards the sensor. It is conceivable, that this is due to the texture of the façades. However, there are at least some PS located on the skyscraper at the top of the SAR image (see Figure 1 and Figure 2), whose façade looks quite similar as can be seen from the oblique view aerial image displayed in Figure 8.

4. CONCLUSIONS

In theory a SAR simulator can assist the PSI analysis by helping to determine the exact location of the PS. This is true, if very precise and detailed 3D building models are available. Although 3D building models are available for many urban areas, they seldom contain the geometry of the façades. The façade is mostly represented with an image texture, which is feasible for visualization purposes, but not for SAR simulation. To simulate the façade reflection, a 3D model containing the façade geometry is necessary.

However, the simulation still proved to be useful. We could demonstrate that the double bouncing between building and ground does not cause many PS. Most PS in our test scene are caused by scatterers located on the building roofs.

Without highly detailed building models, SAR simulation can only provide very rudimentary assistance for the PSI analysis. In future work we will augment the 3D model by close range Photogrammetry in order to represent also pillars, doors, windows and balconies. In a next step we want to group PS and match those against facade structures.

ACKNOWLEDGEMENTS

Part of the work was supported by the Research Fellowship for International Young Scientists of the National Natural Science Foundation of China (Grant No. 60950110351).

REFERENCES

- Auer, S., Hinz, S., and Bamler, R., 2010. Ray-tracing simulation techniques for understanding high-resolution SAR images. *IEEE Transactions on Geoscience and Remote Sensing* 48(3), pp. 1445-1456.
- Bamler, R., Eineder, M., Adam, N., Zhu, X., Gernhardt, S., 2009. Interferometric Potential of High Resolution Spaceborne SAR. *Photogrammetrie - Fernerkundung - Geoinformation* 5, pp. 407-419.
- Becker, S., 2009. Generation and application of rules for quality dependent facade reconstruction. *ISPRS Journal of Photogrammetry and Remote Sensing* 64, pp. 640-653.
- Ferretti, A., Prati, C., Rocca, F., 2000. Nonlinear subsidence rate estimation using permanent scatterers in differential SAR interferometry. *IEEE Transactions on Geoscience and Remote Sensing* 38(5), pp. 2202-2212.

Ferretti, A., Prati, C., Rocca, F., 2001. Permanent scatterers in SAR interferometry. *IEEE Transactions on Geoscience and Remote Sensing* 39(1), pp. 8-20.

Franceschetti, G., Migliaccio, M., and Riccio, D., 1995. The SAR simulation: an overview. In: *Proc. IGARSS 1995*, Florence, 1995.

Hooper, A., Segall, P., Zebker, H., 2007. Persistent scatterer InSAR for crustal deformation analysis, with application to Volcán Alcedo, Galápagos. *Journal of Geophysical Research* 112.

Liu, G., Buckley, S., Ding, X., Chen, Q., Luo, X., 2009. Estimating Spatiotemporal Ground Deformation With Improved Permanent-Scatterer Interferometry. *IEEE Transactions on Geoscience and Remote Sensing* 47(8), pp. 2762-2772.

NVIDIA, 2009. NVIDIA OptiX Ray Tracing Engine. Programming Guide. Available online: <http://developer.nvidia.com/object/optix-home.html>. [last accessed on June 4, 2010]

Zribi, M., Baghdadi, N., and Guérin, C., 2006. A new semi-empirical model for the analysis of surface roughness heterogeneity. In: *Proc. IGARSS 2006*, Denver, Colorado, 2006.